International Journal of Thermophysics, Vol. 14, No. 3, 1993

Time-Resolved X-Ray Scattering Studies of Rapid Crystallization of Amorphous Metals[1]

S. Brauer,[2,3] H. E. Fischer,[2,4] J. O. Ström-Olsen,[2] M. Sutton,[2] and G. B. Stephenson[5]

Time-resolved X-ray scattering has been used to study the kinetics of crystallization of amorphous metals on time scales varying from minutes to milliseconds. Measurements have been at the National Synchrotron Light Source, using a wide-bandpass monochomator and fast linear position-sensitive detector system at the IBM/MIT beamline X-20C. With this apparatus, scattering patterns from the transforming material can be acquired with 3-ms time resolution. A fast pyrometric temperature controller has been developed to change and regulate the sample temperature with microsecond response. In a typical measurement, two synchronized position-sensitive detectors provide complementary *in situ* information about the transformation. The first is used for wide-angle scattering and allows us to determine which phases are present and to what extent. Changes in lattice parameter and particle size can also be deduced. The second detector measures small-angle scattering, yielding additional information about the microstructure, such as the spacing between lammellae in eutectic systems. At relatively slow transformation rates, quantitative measurements of crystal volume fractions as small as 10^{-4} are possible. In many systems, as the transformation rate is increased, the crystallization mechanism changes such that new metastable crystal phases are formed en route to the equilibrium structure.

KEY WORDS: amorphous metals; crystallization; *in situ* measurements; X-ray scattering.

[1] Paper presented at the Third Workshop on Subsecond Thermophysics, September 17–18, 1992, Graz, Austria.

[2] Centre for the Physics of Materials and Department of Physics, McGill University, 3600 University Street, Montréal, Québec H3A 2T8, Canada.

[3] Present address: IBM Research Division, T. J. Watson Research Center, P.O. Box 218, Yorktown Heights, New York 10598, U.S.A.

[4] Present address: LURE, Bâtiment 209D, Centre Universitaire Paris-Sud 91405, Orsay Cedex, France.

[5] IBM Research Division, T. J. Watson Research Center, P.O. Box 218, Yorktown Heights, New York 10598, U.S.A.

0195-928X/93/0500-0541$07.00/0

1. INTRODUCTION

Many interesting nonequilibrium properties of materials occur on time scales which are experimentally challenging to study. To meet this challenge, much work has been devoted in recent years to developing fast optical, thermal, and electron transport measurements. These measurements are commonly used to infer the structural changes which occur during rapid phase transformations. Using rapid data acquisition, these techniques commonly achieve a time resolution on the microsecond scale. In this paper we discuss recent developments in the use of time-resolved X-ray scattering, whereby we can make rapid structural measurements directly. With this technique, a sequence of diffraction patterns is recorded in real time, to follow the phase evolution *in situ*. The time resolution is limited by the time required to accumulate each diffraction pattern. With conventional X-ray sources and single-channel detectors, the time to obtain a diffraction pattern ranges from minutes to days. By using array detectors and the new synchrotron X-ray sources, this time can be reduced to milliseconds [1].

2. METALLIC GLASSES

In this paper, we demonstrate our time-resolved scattering technique with examples from our study of metallic glass crystallization. Metallic glasses are formed by cooling liquid metal alloys rapidly enough to prevent the formation of any crystalline order. This leaves the alloy in a thermally arrested metastable state. When heated, a rich assortment of nonequilibrium phenomena occurs as the material transforms to its equilibrium phase(s). Apart from the technological interest in understanding these transformations, metallic glass crystallization is an ideal forum for investigating solid-state nucleation and growth into an isotropic medium. This is partly because the process can be much more easily controlled than, for example, solidification from the melt.

Metallic glass crystallization is classified into three types depending on the crystal phases which are formed [2]. The simplest type, called polymorphic crystallization, occurs when the crystal phase has the same composition as the glass. Diffusion of material over long distances is not required since the crystal phase can be formed by only local atomic rearrangements. A more complicated type, called primary crystallization, occurs when the composition of the crystal phase is different from the starting composition. As primary crystallization proceeds, the remaining amorphous phase changes composition with time, and it eventually crystallizes into another phase of different composition. The third type is called

eutectic crystallization and involves the simultaneous formation of two crystal phases with the correct compositions so as to leave the amorphous material at its original composition. Such a transformation involves diffusion on length scales of hundreds of angstroms. The resulting microstructure is often lamellar, i.e., composed of alternating layers of the two crystal phases.

For all of these reactions, the time scale of crystallization can be varied over a wide range by changing the transformation temperature. For a particular alloy, at low transformation rates, crystallization may proceed directly to the equilibrium structure(s) on the phase diagram. In many cases, however, more rapid crystallization results in several competing transformations through which other metastable phases are temporarily formed [3]. *In situ* time-resolved diffraction provides an ideal tool for investigating these rapid irreversible processes. The appearance and disappearance of phases can be monitored on the millisecond time scale, to give a qualitative understanding of the transformation process. Furthermore, it is possible to measure the amounts and morphologies of the various phases. This allows quantitative comparison to theoretical models of the kinetics. In the paper, we give examples from each of the three crystallization mechanisms in turn, to demonstrate the different types of information which can be obtained.

3. EXPERIMENTAL METHODS

In a typical experiment, crystallization is brought about by abruptly heating a specimen from room temperature to a prescribed transformation temperature. X-ray diffraction patterns are repeatedly acquired as the system evolves toward thermodynamic equilibrium at the new temperature.

The experiments are conducted at the National Synchrotron Light Source (NSLS) with the IBM/MIT beamline X-20C which has been optimized for time-resolved scattering measurements. Detailed descriptions of our experimental setup have been published previously [1, 3]. This bending-magnet beamline is equipped with a platinum-coated silicon 1:1 focusing mirror which collects 4 mrad of synchrotron radiational and focuses it to a 2×1-mm spot at the sample position, 22 m from the source. A double crystal monochromator is used to select the X-ray wavelength in the range of 1.5 to 2.0 Å. The crystals are in fact synthetic multilayers of tungsten and silicon, which provide a broad energy bandpass of 1% full width at half maximum (FWHM). This greatly increases the incident X-ray intensity, with a corresponding resolution loss which is unimportant for these studies. The net resolution ($\Delta q/q = 0.015\text{FWHM}$) is a convolution of the energy resolution with a geometrical contribution resulting from the

finite beam size on the sample. The beamline is evacuated, the X-rays passing through Be windows at each end. At a typical synchrotron ring current of 100 mA, an incident intensity of 10^{13} photons per second is obtained.

Figure 1 depicts the experimental configuration downstream from the beamline. X-rays pass through two sets of horizontal and vertical slits and a beam monitor before striking the specimen. Scattered X-rays are detected with two linear-array position sensitive detectors (PSDs), which provide complementary information about the transformation. The first detector measures wide-angle X-ray scattering (WAXS), revealing Bragg peaks of the crystal phase(s), as well as broad scattering from the amorphous material. Typically, this detector array spans $\Delta(2\theta) = 15 - 20°$. The other detector measures small-angle scattering (SAXS) to probe microstructural changes on much longer length scales. Each PSD consists of a 25-mm-long photodiode array containing 1024 pixels. The pixels can be electronically grouped to improve time resolution at the expense of spatial resolution. In a 1024-pixel configuration, diffraction patterns can be collected as quickly as every 16 ms; 64-pixel patterns take 3 ms.

The samples are melt-spun ribbons of amorphous alloy, typically 20 μm thick, 1.5 mm wide and 2.5 cm long. They are clamped at each end to water-cooled electrical contacts and heated resistively by passing a direct current along the sample length. When the sample chamber is evacuated, the geometry results in a several-millimeter-long central region where the temperature is constant to ± 2 K. To take up the length change due to thermal expansion and to keep the ribbon flat, one contact is spring-loaded to apply a small tension to the sample. By recording the sample voltage and current, the power input to the specimen and the overall resistance are obtained as a function of time, with 10 times greater time resolution than the diffraction data.

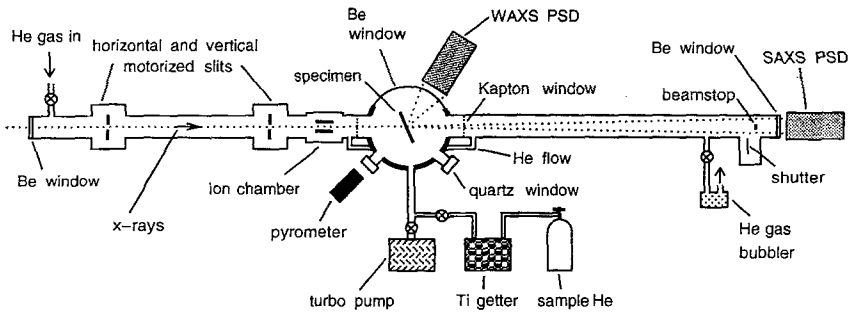

Fig. 1. Schematic diagram of the experimental setup showing the X-ray scattering geometry.

Careful temperature control is critical to the success of these experiments. For the transformation to be considered isothermal (which greatly simplifies any quantitative analysis of the results), the transient in the temperature step must be much shorter than the phase transition time. To take full advantage of the available X-ray diffraction time resolution, it was necessary to develop techniques to change sample temperature by hundreds of degrees in milliseconds in a uniform and controlled manner. These goals are complicated by the change in sample resistance and the release of latent heat during the transformation. The pyrometric temperature controller which was designed for this purpose is described in a recent publication [4]. This device can be used to heat samples from room temperature to 600–800 K, without overshoot, in approximately 1 ms. The temperature is held constant thereafter until the transformation is complete. For crystallization times in excess of 15 s, the sample chamber was evacuated to $\approx 10^{-3}$ Pa. However, $\frac{1}{3}$ of an atmosphere of 99.9999% purity He was backfilled into the chamber to help remove the latent heat during faster runs. When this is done, the gas preferentially cools the sample edges so that temperature gradients are formed across the 1.5-mm width of the ribbons. This gradient is exacerbated during the crystallization because of the relatively large resistivity change. As the hotter central region crystallizes more rapidly, more of the electrical power is dissipated there, increasing the nonuniformity. During these runs, the horizontal X-ray beam size is reduced using the slits, to illuminate only the central 0.2 mm of the sample width. In this way, the temperature can be kept constant to ± 2 K throughout the scattering volume. The pyrometer was calibrated by comparing the kinetics observed at slow rates with the kinetics observed during crystallization measurements made with a differential scanning calorimeter (DSC). The absolute temperature could then be established to ± 5 K. We note that the present limit to isothermal crystallization rate is determined by the dissipation of latent heat, which disrupts the temperature uniformity during very rapid crystallization. The fastest isothermal crystallization time (i.e., time until half-crystallized) is typically a few hundred milliseconds [5].

4. POLYMORPHIC CRYSTALLIZATION

Figure 2 shows a sequence of WAXS diffraction patterns for different times during slow polymorphic crystallization of Co_2B at 729 K. The initial $t = 0$ s pattern is the characteristic broad scattering of the glass. As time increases, Bragg peaks of the equilibrium crystal phase grow in intensity and the broad amorphous background decays until, at the end, only scattering from the crystal phase is observed. For these data, the width of the

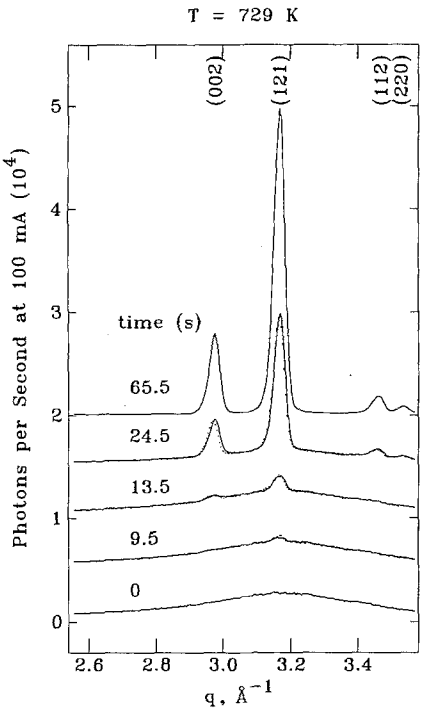

Fig. 2. Time-resolved X-ray scattering patterns for Co_2B at $T = 729$ K. The time per diffraction pattern is 0.275 s. For clarity, only 5 of the 400 measured patterns are shown, shifted vertically by even increments. Since the intensity of X-rays from a synchrotron changes with time, all intensities have been normalized to a ring current of 100 mA.

Bragg peaks is set by the resolution limit. Since the intensity of X-rays from a synchrotron changes with time, all intensities have been normalized to ring current of 100 mA. The X-ray ring at NSLS typically operates between 150 and 250 mA. In Fig. 2, the time to collect each diffraction pattern was 0.275 s, and only 5 of the 400 collected patterns are shown.

To extract the crystallized volume fraction from these data, the scattering patterns were fit as a linear combination of the amorphous scattering $I_A(q)$ and crystalline scattering $I_C(q)$. Explicitly, the scattering intensity for a given wavenumber q and time t is

$$I(q, t) = [1 - X(t)]\, I_A(q) + X(t)\, I_C(q) \tag{1}$$

where $X(t)$ is the volume fraction of crystallites. The model is reasonable since the scattering intensity of each phase is proportional to the volume of material giving rise to that scattering, provided the scattering pattern of each phase does not change with time. For the Co_2B data, $I_A(q)$ and $I_C(q)$ were the measured scattering patterns at the initial and final times, respectively. This procedure implicitly tests whether the increase in crystalline scattering is compensated for by a corresponding loss of amorphous scattering. Any systematic deviations of the model from the data directly indicate when the model breaks down.

As represented by the solid lines in Fig. 2, this simple one-parameter model provides a good description of the data. The volume fraction measurements so obtained are shown in Fig. 3. Note that crystal volume fractions of a few parts per 10^4 can be deduced. (With yet slower crystalization, longer integration times provide sufficient counting statistics that one part in 10^4 is easily resolved.) This high sensitivity is possible because our analysis compares intermediate scattering patterns to the initial and final states, all taken under identical thermal and geometric conditions, so that

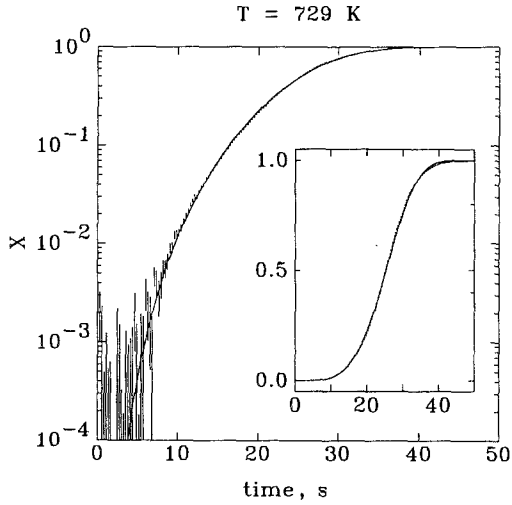

Fig. 3. The time evolution of crystalline volume fraction (X) for Co_2B at $T = 729$ K. The error bars indicate the uncertainty resulting from the least-squares fit of the data in Fig. 2 with Eq. (1). The solid line is a fit to a simple nucleation and growth model which predicts $X(t) = 1 - \exp(\alpha t^4)$. The constant α depends on the nucleation and growth rates, and in this case $\alpha = 2.1 \times 10^{-6}\,s^{-4}$. Inset: The same data ona linear scale.

the measurement is effectively differential. The volume fraction results were themselves fit using a simple nucleation and growth model [6], which is also plotted in the figure to show how kinetic parameters can be obtained from the data.

For Co_2B, only the equilibrium crystal phase is formed, even at the fastest isothermal transformation rates which we have studied. Because of this simple behavior, we have used this model alloy to investigate crystallization kinetics over a wide range of time scales [7]. This single-phase crystallization is contrast to most of the polymorphic transformations which we have investigated. For example, the well-known glass $NiZr_2$ transforms to the equilibrium crystal phase of that composition at low transformation rates but forms an increasing fraction of a new metastable crystal phase at higher rates. Quantitative measurements of the volume fractions of the two phases were obtained by fitting the scattering patterns with an extended version of Eq. (1):

$$I(q, t) = [1 - X(t) - Y(t)]\, I_A(q) + X(t)\, I_{C1}(q) + Y(r)\, I_{C2}(q) \qquad (2)$$

where $X(t)$ and $Y(t)$ are the volume fractions of equilibrium (C(1) and metastable (C2) crystal phases, respectively. The results are shown in Fig. 4 for three different annealing temperatures. The new metastable phase $Y(t)$ forms before the equilibrium phase $X(t)$ in each case, a trend which is more pronounced at higher temperatures. One of the advantages of our technique is that, by terminating the sample heating power, we can rapidly quench partially crystalline samples for subsequent structural analysis. In this way, the new metastable crystal phase of $NiZr_2$ has been identified [3].

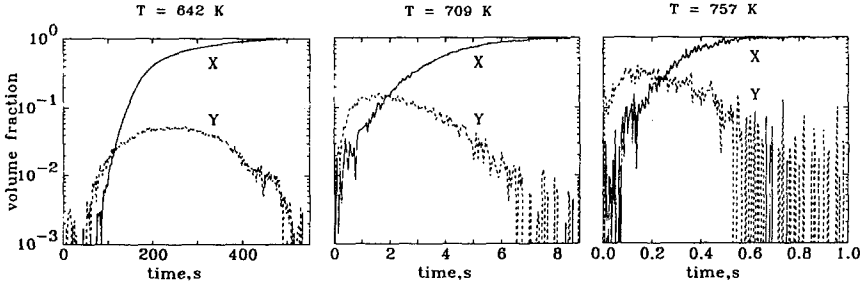

Fig. 4. Volume fractions of the equilibrium (X) and new metastable (Y) crystal phases of $NiZr_2$, during polymorphic crystallization at $T = 642$, 709, and 757 K. Formation of the new metastable phase precedes that of the equilibrium phase, a trend which becomes more pronounced with increasing anneal temperature.

5. PRIMARY CRYSTALLIZATION

The primary crystallization of a recently developed metallic glass alloy called Finemet (Fe–Cu–Nb–Si–B) demonstrates how additional structural and microstructual information can be obtained using time-resolved WAXS [8]. This alloy crystallizes by precipitating very fine (~400-Å-diameter) α-Fe particles, thereby forming an excellent soft magnetic material. During isothermal crystallization, as shown in Fig. 5, the α-Fe (110) peak grows at the expense of the broad amorphous background.

Figure 6a shows the crystalline volume fraction as a function of time, obtained by fitting the data in Fig. 5, again using Eq. (1). However, from Fig. 5 it is clear that the α-Fe peak narrows as it grows. To allow for this, the final crystalline scattering pattern $I_C(q)$ was taken to be a Gaussian line-shape, fit to the final α-Fe peak. With this approach, the width of the Bragg peak as a function of time could also be extracted from the data. (The area under the Gaussian line-shape was conserved when the width was changed.) The peak width (corrected for instrumental resolution) was then used to calculate the mean crystal diameter as a function of time (Fig. 6b), via the Scherrer formula [9]. The results agree with subsequent transmission electron microscopy observations. The ratio of the transformed volume to the mean crystallite volume is a measure of the number

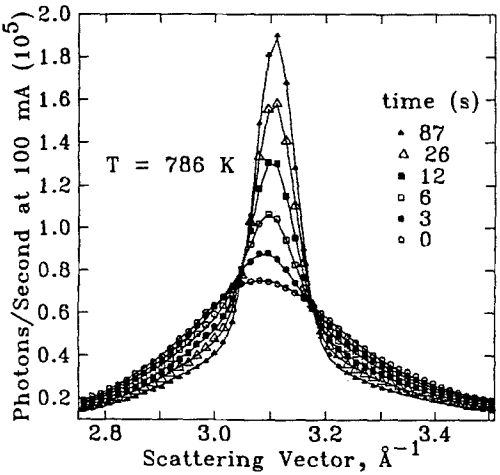

Fig. 5. Time-resolved wide-angle scattering from the metallic glass Finemet, undergoing primary crystallization at $T = 786$ K. Solid lines through the data are fits which were used to extract the crystal volume fraction, mean particle size, and average lattice constant as functions of time.

of crystals formed. Nucleation and diffusion-controlled growth models can be tested with these results. The measured growth rate can be used to deduce the limiting diffusion constant.

Careful examination of Fig. 5 also reveals a clear shift in the α-Fe peak position during the transformation. To account for this, the position of the Gaussian peak was also allowed to vary during the fits. The BCC lattice parameter was then calculated, as a function of time, and is shown in Fig. 6c. We attribute the peak shift to the diffusion of the larger Nb atoms out of the α-Fe crystals during growth.

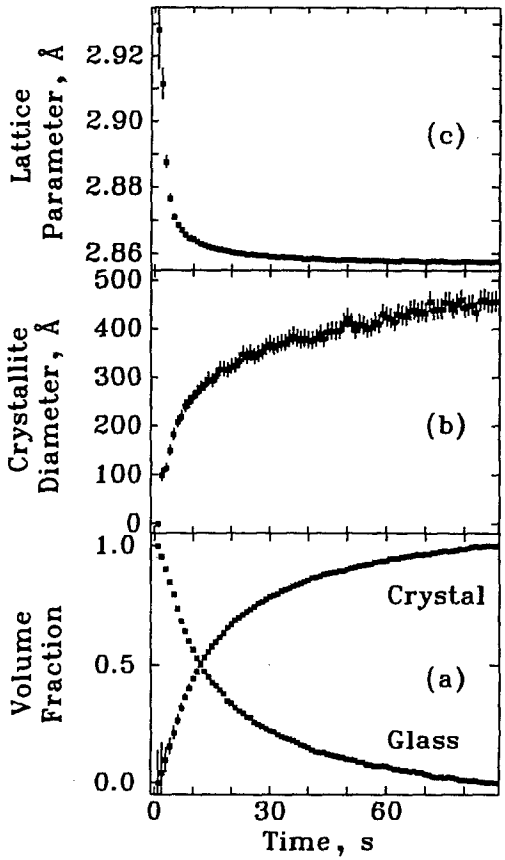

Fig. 6. The time evolution of volume fractions (a), mean crystallite diameter (b), and BCC lattice parameter (c), obtained by fitting the data in Fig. 5 as described in the text.

6. EUTECTIC CRYSTALLIZATION

Figure 7 shows the large-angle data for isothermal eutectic crystallization of $Co_{92}Zr_{08}$ (8.03 atomic% Zirconium) at $T \approx 850$ K. For this alloy, the two phases β-Co and Co_5Zr grow simultaneously from the glass. The occurrence of well-separated peaks for (200) β-Co (not shown) and (220) Co_5Zr allows us to monitor the evolution of these two phases independently. Their volume fraction ratio remains relatively constant during crystallization, as expected. The weak central peak is due to the formation of a small amount of α-Co.

The SAXS data for the same run are displayed in Fig. 8. For this data run, a total of 400 LAXS and SAXS diffraction patterns was taken, the patterns being separated by 26 ms. The well-defined peak at about $q = 0.03$ Å^{-1} corresponds to the eutectic formation of β-Co and Co_5Zr with an interlamellar spacing of about 200 Å. It is also apparent that this SAXS peak gradually moves toward lower q values during crystallization, indicating that the eutectic length scale is somewhat smaller at earlier times.

From the large-angle data we can measure the order of appearance of the phases and the relative volume fractions. From the small-angle data we can study the evolution of the eutectic microstructures. By making these

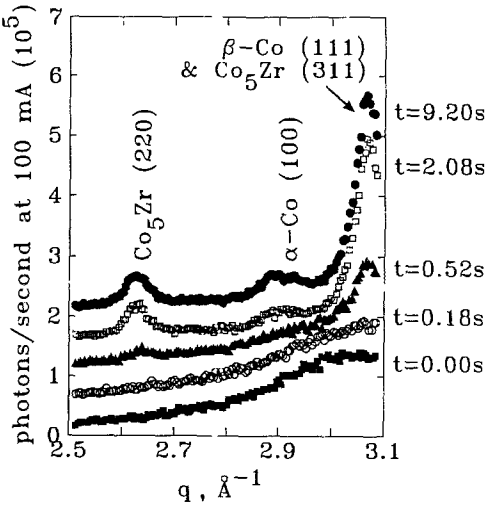

Fig. 7. Wide-angle scattering patterns obtained during eutectic crystallization of $Co_{92}Zr_{08}$ at $T \approx 850$ K. The peak at 3.05 Å^{-1} is the superposition of the (311) peak of Co_5Zr and the (111) peak of β-Co.

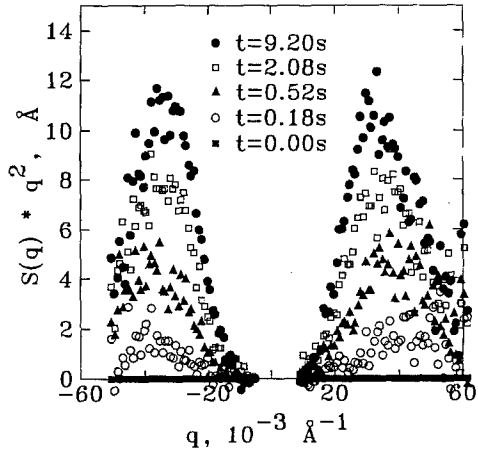

Fig. 8. Small-angle scattering (SAXS) for the same data run as shown in Fig. 7. The position of the SAXS peak indicates a eutectic interlamellar spacing of about 200 Å.

measurements at several compositions around the eutectic composition and at several temperatures, we will be able to test theories for the time evolution of eutectic crystallization. We will also be able to investigate the crossover from eutectic to primary crystallization. The ability to measure both large- and small-angle scattering simultaneously is essential to these studies.

7. CONCLUSIONS

These results demonstrate the remarkable ability of time-resolved scattering experiments to reveal, *in situ*, the intricate behavior of structural phase transformations. Application of this technique to the study of metallic glass crystallization reveals a particularly diverse collection of interesting nonequilibrium phenomena.

At the moment, the time scale of rapid crystallization studies is limited by two factors. Isothermal conditions greatly simplify any quantitative analysis of these results. However, with our thermal geometry and temperature control, the release of latent heat limits isothermal crystallization times to a few hundred milliseconds. To improve on this, we must solve the challenging experimental problem of increased cooling power while maintaining temperature uniformity. Alternatively, techniques can be developed for analyzing nonisothermal crystallization kinetics [10]. The second limitation is X-ray flux. At our fastest sampling rates (3 ms), we can com-

monly collect a few hundred counts per pixel in a Bragg peak. Particularly when multiple phases are involved, greater signals would be beneficial for deciphering the phases and monitoring the kinetics. Given the growing interest in time-resolved X-ray scattering, we are confident that brighter synchrotron sources and yet faster detector systems will make microsecond-resolution structural studies common in the near-future.

REFERENCES

1. G. B. Stephenson, K. F. Ludwig, Jr., J. L. Jordan-Sweet, S. Brauer, F. Mainville, Y. S. Yang, and M. Sutton, *Rev. Sci. Instrum.* **60**:1537 (1989).
2. U. Köster and U. Herold, in *Glassy Metals I*, H.-J. Güntherodt and H. Beck, eds. (Springer-Verlag, New York, 1981), Chap. 10.
3. S. Brauer, J. O. Ström-Olsen, M. Sutton, Y. S. Yang, A. Zaluska, GH. B. Stephenson, and U. Köster, *Phys. Rev. B* **45**:7704 (1992).
4. S. Brauer, D. H. Ryan, J. O. Ström-Olsen, M. Sutton, and G. B. Stephenson, *Rev. Sci. Instrum.* **61**:2214 (1990).
5. S. Brauer, H. E. Fischer, J. O. Ström-Olsen, M. Sutton, and G. B. Stephenson, in *National Sunchrotron Light Source Annual Report*, S. L. Hulbert and N. M. Lazarz, eds. (1990), pp. 311.
6. J. W. Christian, *Transformations in Metals and Alloys*, 2nd ed., part I (Pergamon, Oxford, 1975).
7. S. Brauer, H. E. Fischer, J. O. Ström-Olsen, M. Sutton, A. Zaluska, and G. B. Stephenson, in press.
8. U. Köster, U. Schünemann, M. Blank-Bewersdroff, S. Brauer, M. Sutton, and G. B. Stephenson, *Mater. Sci. Eng.* **A133**:611 (1991).
9. B. D. Cullity, *Elements of X-ray Diffraction*, 2nd ed. (Addison–Wesley, New York, 1978).
10. U. Köster, U. Schünemann, G. B. Stephenson, S. Brauer, and M. Sutton, *Mater. Res. Soc. Symp. Proc.* **205**:233 (1992).